Numerical Analysis of SSME Preburner Injector Atomization and Combustion Processes

P. Y. Liang,* R. J. Jensen,* and Y. M. Chang†
Rockwell International/Rocketdyne Division, Canoga Park, California

The coaxial spray injection and combustion flowfields of a Space Shuttle Main Engine preburner injector element have been analyzed using a three-phase numerical code, with the objective of defining the flame characteristics and obtaining the temperature profiles at various locations downstream. The former is crucial for delineating the factors that control combustion instability and efficiency, whereas the latter is important for ensuring that temperature nonuniformities are within the design limits as the hot gas enters the turbine nozzles. The model is unique in its comprehensiveness of the physics that are incorporated, which include the processes of atomization, evaporation, secondary droplet breakup, multispecies chemistry, and turbulent diffusion. The model produced realistic results of the complex flowfield, yielding information on the liquid jet length, spray shape, flame zone size and characteristics, and droplet properties. The temperature levels are generally in agreement with the available test data. An external group combustion -type of flame is predicted. Salient combustion and mixing features are discussed, and sources of uncertainty are pointed out for future studies.

Nomenclature

D	= diffusivity
G	= body force
h	= specific enthalpy
I	= specific internal energy; identity matrix
K	= thermal conductivity
P	= pressure
r	= radial coordinate = x if cylindrical, = 1 if two-dimensional
S	= droplet momentum coupling term
t	= time
T	= temperature
u, v, w	= gas velocity components
y	= axial coordinate or species mass
μ, λ	= viscosity
ρ	= density
σ	= viscous stress tensor
τ	= stress deviator for swirl component
∇	= differentiation operation, $i\frac{\partial}{\partial x}+j\frac{\partial}{\partial y}$

Subscripts

$\approx$	= tensor quantity
k	= species number

Introduction

THE Space Shuttle Main Engine (SSME) high-pressure fuel preburner consists of 264 coaxial injector elements injecting gaseous hydrogen and liquid oxygen into a large cylindrical chamber. Primary atomization is caused by the large velocity gradient between the fuel and oxidizer streams. Under supercritical conditions, the LOX droplets then undergo secondary atomization and evaporation, which are believed to be the rate-controlling steps in the overall combustion process. The reacted gases then feed into a convergent section that leads to the turbine that drives the fuel pump. This complex multistage process needs to take place within well-defined operating and physical limits to ensure that certain flowfield characteristics, notably the temperatures, do not exceed the design specifications of the confining structure and downstream turbine. Up to now, the only sure means to ascertain the proper performance of the injector/combustor has been cut and try testing. The need to understand the flowfield without having to rely solely on hot-fire measurements is obvious. Furthermore, the SSME is continually being upgraded and modified to improve its life and performance. Thus, an analytical means of assessing the effects of design changes without resorting to expensive experimentation is greatly desired. This study represents a first attempt to simulate the multiphase reactive turbulent flowfield from first principles. While much ongoing research is still trying to verify the accuracy of the numerics and to reduce the degree of empiricism in the physics of submodels, it has been the intent of this study to include all of the major physical mechanisms important to spray combustion. Thus, the process of liquid jet atomization itself is modeled in conjunction with droplet evaporation, heatup, and secondary droplet breakup. This is in contrast with most other previous studies of spray combustion flames that take the completely atomized spray as an input or simply treat the spray as a gas (e.g., Refs. 1-3). Furthermore, all of the processes are solved in a coupled fashion, together with the chemical source terms and the fluid dynamics. The liquid jet, the droplets, and the multispecies gas mixture are all assumed to displace nonnegligible volumes in the same vicinity, in particular, in the same computational cell.

The Advanced Rocket Injector Combustor Code (ARICC)[4] used in the present analysis was originally developed to simulate these types of flowfields. With a true coupled three-phase capability and a modular structure to allow for the incorporation of various physical models, realistic simulations of the complete combusting flowfield and accompanying processes were made. Two geometries were studied. As shown in Fig. 1, both of these are slight variations of a basic coaxial injector element with a cup recess design. The first design corresponds to a prototype SSME injector element for which there are some actual hot-fire test results that can be used for the validation of computed data. The second is the production SSME preburner injector geometry. The major difference is the 7-deg tapered injector tip, which was incorporated on the production injector to decrease the pressure drop. The main features of the current model will be briefly described in the next section, and then the results and analysis of the present study will be discussed in the third section.

Numerical Code and Enhancements

ARICC is a transient finite-difference code for multispecies reacting flows where a liquid phase and particulate droplets

Presented as Paper 86-0454 at the AIAA 24th Aerospace Sciences Meeting, Reno, NV, Jan 6-9, 1986; received Feb. 4, 1986; revision received Feb. 1, 1987.

*Member of Technical Staff, Combustion Devices.
†Project Engineer, Flow Systems Analysis.

are also present and interact with each other. The major advancement represented by the development of ARICC is in its ability to handle all three phases together. This ability is deemed necessary for the simulation of the coaxial injector flows where atomization takes place over an extended region and both the liquid and droplet phases occupy significant volumes. The mathematical framework consists of a hybrid Eulerian/Lagrangian approach adapted to function with both incompressible and compressible fluids simultaneously. The governing equations, which include the full axisymmetric/two-dimensional Navier-Stokes equations with swirl, and the solution procedure, are presented in detail in Ref. 5. Only the major equations are summarized here for completeness' sake.

The mass conservation for the kth species of the gaseous mixture is given by

$$\frac{\partial \rho_k}{\partial t}+\frac{1}{r}\nabla\cdot(r\rho_k u)=\underbrace{\frac{1}{r}\nabla\cdot[r\rho D\nabla(\rho_k/\rho)]}_{\text{diffusion}}+\underbrace{\dot{\rho}_k^c}_{\text{chem}}+\underbrace{\dot{\rho}_s\delta_{k1}}_{\text{evap}} \tag{1}$$

where species 1 is assumed to be the spray species. The same equation reduces to

$$\frac{1}{r}\nabla\cdot(ru)=0 \tag{2}$$

for the incompressible liquid jet. Momentum conservation for both the liquid and the gas is given by

$$\frac{\partial(\bar{\rho}\underset{\sim}{u})}{\partial t}+\frac{1}{r}\nabla\cdot(r\bar{\rho}\underset{\sim}{u}\underset{\sim}{u})=-\nabla P+\frac{1}{r}\nabla\cdot(r\underset{\approx}{\sigma})$$

$$-\frac{(\sigma_0-\bar{\rho}w^2)}{r}\nabla r+S+\bar{\rho}G \tag{3}$$

where σ and σ_o are viscous force terms. Thirdly, the conservation for internal energy is given by

$$\frac{\partial(\rho I)}{\partial t}+\frac{1}{r}\nabla\cdot(r\rho I\underset{\sim}{u})=-\frac{P}{r}\nabla(r\underset{\sim}{u})+\underset{\approx}{\sigma}:\nabla\underset{\sim}{u}+\tau\cdot\nabla(w/r)$$

$$+\frac{\sigma_0}{r}\underset{\sim}{u}\cdot\nabla r-\frac{1}{r}\nabla\cdot(r\underset{\sim}{J})+\underbrace{\dot{Q}_c}_{\text{chem}}+\underbrace{\dot{Q}_s}_{\text{evap}} \tag{4}$$

where J includes the heat flux due to conduction and species diffusion:

$$\underset{\sim}{J}=K\nabla T-\rho D\sum_k h_k\nabla(\rho_k/\rho) \tag{5}$$

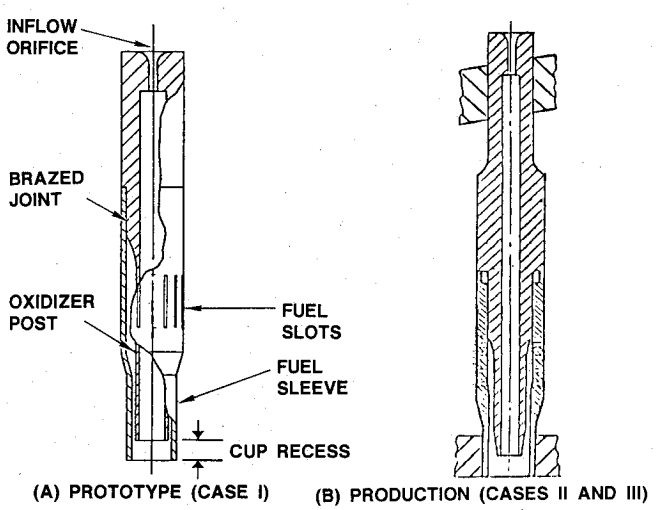

Fig. 1 Schematic of SSME injector elements.

To solve for the liquid and gas flowfields, these equations are then turned into typical finite-volume difference equations with an Eulerian curvilinear mesh with a "staggered grid" convention, i.e., having the velocities defined at the vertices of the control cell volumes and all the other variables defined at the cell centers. The solution procedure is a modified time-marching three-step implicit continuous Eulerian[6] (ICE) technique that first solves for all the Lagrangian terms in the momentum and energy equations explicitly. Then, combining the continuity and momentum equations, a Newton-Raphson type of point successive over relaxation (SOR) is carried out on the pressure term to obtain an implicit solution. The energy terms are also adjusted to reflect the implicit results. Finally, the convective terms are solved to produce the Eulerian solution. The interfaces between the liquid and the gas are described with a volume of fluid (VOF) technique.[5] The complex physics of the problem are embedded mostly in the many source terms of the governing equations, which are solved independently in different submodules of the program. Some source terms involve information from the spray droplets, which are tracked as discrete particles in a purely Lagrangian fashion once they have been created by the atomization process. Drop turbulent dispersion is accounted for by a random walk model. Thus, the current treatment of the spray falls into the so-called SSF type of approach.[7]

In solving for the convective terms, a user-controlled amount of spatial upwind differencing is used to ensure stability. (Zero upwind differencing means centered differencing that is unstable.) In the present series of runs, pure upwind differencing is used, which represents the single most important source of numerical diffusion. (A small amount of so-called "antinode coupling" is also used to suppress short wavelength velocity oscillations peculiar to the ICE method. This represents an additional minor source of artificial viscosity.) Since the amount of numerical diffusion from this source is somewhat grid-dependent, a limited-length test case with three times as much grid resolution radially compared with the standard grid used for the "production runs" was made for the SSME Phase II$^+$ conditions (see following section). The results from this test run indicate that while better resolution of the shear layer near the injector tip region is achieved by the finer grid, the overall qualitative features of the flame and flowfield are not significantly affected. Since the primary objective of the present study is to demonstrate capability and determine the cross-sectional temperature profiles far downstream, it was deemed not worth the extra cost to use the finer grid. This is not to say, however, that numerical diffusion is insignificant or that discretization effects have been asymptotically eliminated. Indeed, an order of magnitude study[8] has been performed, reminding us of the need to interpret any modeling results with these effects in mind. Rather, the current insensitivity of the qualitative features to grid resolution stems from the fact that the gaseous flowfields under study are dominated by the rate-controlling processes of drop vaporization and secondary breakup, which in turn are related to droplet penetration. Thus, for furthering the current studies, the top priorities are gaining additional knowledge about dropsize distribution and improving the atomization and breakup models.

Since the code's inception, however, a number of improvements[9] in the physical models have been incorporated. The importance of taking these refinements into consideration is discussed in Refs. 10–13. They are summarized in Table 1. The need for these enhancements stems primarily from two factors: 1) the characteristics of a "dense" spray as contrasted with a typical "thin" spray, and 2) the supercritical conditions under which the liquid oxygen (LOX) droplets spend most of

Table 1 Summary of special physical models used in upgraded ARICC

Feature	Reason needed	Refs.
A) Variable drop densities -large drop volumes	Dense/supercritical spray	10,11
B) Variable C_D	Drop deformation	11,12
C) Stripping evaporation	Secondary drop breakup	14,15
D) Supercritical drop properties	Supercritical pressure and temperature	10,13

their lifetime—while still being treated as coherent entities. These "droplets" undergo tremendous changes in density as they approach the critical point (feature A of Table 1). The resulting prospect of droplets taking up a large portion of the volume of a computational cell demanded substantial upgrading of the numerical scheme so that the corresponding small gaseous cell volumes would not result in an unacceptably stiff system—i.e., one that can be solved only in extremely small time steps. This problem is largely overcome through special numerical averaging treatments for such tiny gas pockets, as well as by allowing large colliding drops to coagulate and be reformed into liquid fragments.

Secondly, large droplets moving at a high velocity will also deviate substantially from spherical shapes. Hence variable drag coefficients (feature B) are incorporated. Large drops, and especially supercritical drops without surface tension, tend to break up into tiny fragments that vaporize practically instantaneously.[14] The dominant breakup mode under the high-Reynolds number environment of the present studies is the so-called "shear stripping mode."[15] Thus a "stripping evaporation" model is incorporated in addition to the conventional diffusion evaporation model. Typically, the stripping evaporation rate is an order of magnitude faster than the diffusion evaporation. Finally, item D of Table 1 refers to the usage of curve-fitted LOX vapor pressure and latent heat properties near the critical pressure regime. It should be noted that much measurement of basic physical properties, especially those for multiple-component environments, still remains to be done. Those used only represent the best available extrapolation of data from literature. Such uncertainty affects the validity of the absolute quantitative prediction of some sensitive features in the flowfield such as flame zone thickness or sizes, although a comparative study using consistent models will still generate much physical insight into the problem.

Results and Discussion

A total of three cases have been run using the model. The first one corresponds to the prototype injector geometry (Fig. 1a) and test conditions. The second and the third cases both use the production SSME injector geometry (Fig. 1b), but the flow parameters correspond to the Phase I and Phase II$^+$ operating conditions respectively. The problem parameters for all three cases are summarized in Table 2. Other than geometry, the major difference between case I and cases II and III is that the latter have part of the fuel (gaseous hydrogen) coming out through tiny holes in the faceplate rather than through the annulus. This cold faceplate flow envelopes the combusting coaxial streams and reduces the recirculation zone, thus minimizing the entrainment of hot gas back toward the faceplate. Another design feature worth pointing out is the recess cup used in both geometries. It has been found[16] that the constrained fuel flow in the cup maintains a much higher velocity during the initial contact with the low-speed LOX stream, greatly facilitating the atomization. Much finer drops are thus created in the cup which are crucial in initiating and maintaining the combustion downstream.

Figure 2 shows a portion of the grid for cases II and III. The outer wall is a free-slip boundary that corresponds to the imaginary symmetry surfaces of a streamtube whose diameter is determined based on the average cross-sectional area available to each injector element. Case I was run with a streamtube about 30 cm long, which is the length of the test combustion chamber.[16] The other two cases have models of 17 cm in length, which is the approximate dimension of the preburner combustion chamber. Each case takes about 21,000 CPU seconds on the CYBER 875 to run through to an approximate steady state.

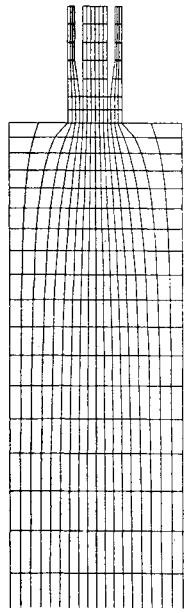

Fig. 2 Computational grid (cases II and III).

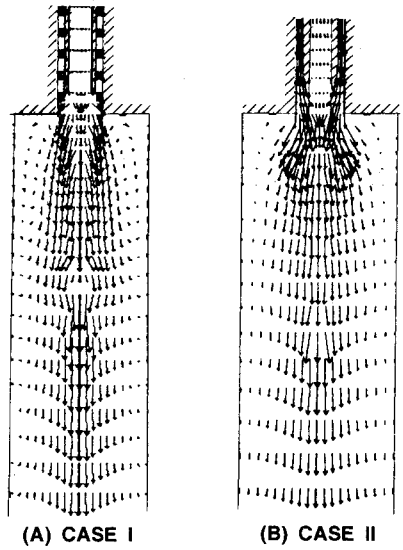

Fig. 3 Velocity vectors of coaxial flowfield.

General Flowfield Features

Figure 3 shows the representative velocity fields of cases I and II. Case III has a qualitatively similar flowfield to case II and is not shown. They both show the rapid expansion and acceleration of the gaseous stream around the centerline driven by the large energy release of the oxygen/hydrogen reaction starting from inside the cup. This accelerating stream in turn enhances the rapid atomization of the center LOX jet (Fig. 4a). The very efficient atomization mechanism results in re-

Table 2 Summary of flow parameters

		Case I	Case II	Case III
Description		SSME Prototype	SSME Phase I	SSME Phase II+
Grid Size		9×61	9×52	9×52
Overall MR		0.83	1.04	0.96
Oxidizer	$\dot{m}$, g/s	149.8	155.4	146.9
(LOX)	$V_{IN.}$, cm/s	2.44×10^3	3.57×10^3	3.38×10^3
	$\rho_{IN.}$, g/cm^3	1.122	1.085	1.085
	$T_{IN.}$, K	106	118	118
Fuel,	$\dot{m}$, g/s	180.5	149.9	153.6
GH_2	$V_{ANNULUS}$, cm/s	2.13×10^4	1.99×10^4	2.20×10^4
	$\rho_{IN.}$, g/cm^3	0.091	0.069	0.069
	$T_{IN.}$, K	69.4	148	148
	V_{BLEED}, cm/s	0	2.16×10^2	1.48×10^2
Exit Boundary Condition		Const. P = 2.41×10^8 dynes/cm^2	Continuative outflow	Continuative outflow

latively short liquid jet lengths, which stand at approximately 1.72 cm for case I and 2.22 cm for case II. (The square of the inflow velocity difference $(V_{g,in}-V_{l,in})^2$, to which the atomization rate is proportional, is about 30% higher for case I than for case II.) Figure 4a also indicates the extent of the spread of the LOX particles. It should be noted that since a droplet group representation is used, the plotted drops do not necessarily reflect the actual density distribution of the spray. However, it is quite apparent that the outward diffusion of the drops is limited, primarily because of their short life span. Figure 4b shows the corresponding gaseous oxygen distribution. As expected, surviving oxygen gas can be found only immediately around the LOX jet itself. Any outwardly diffused oxygen is instantaneously combusted with fuel hydrogen into water and some of the other radicals. The fact that a relatively high oxygen concentration zone does exist, however, indicates that the spray around the centerline is dense enough to cause it to behave as an extended gaseous oxidizer generator, and combustion takes on the characteristics of the group diffusion flame rather than those of multiple flamelets surrounding individual droplet groups. This point will be discussed in the next subsection.

One obvious difference between the flowfields of case I and cases II and III is the presence of a larger recirculation zone in case I (Fig. 3). Some of the hot combusted gases are thus entrained and returned to the faceplate. The use of cold bleed gas through the faceplate alleviates this situation, although the flow downstream becomes more stratified as a cold sheath is formed around the central hot gas.

Spray and Flame Characteristics

The isotherm plots shown in Fig. 5 both display the same basic characteristics. In Ref. 17, it was pointed out that spray combustion can be divided into four regimes: single droplet combustion, internal group combustion, external group combustion, and external sheath combustion, depending on a "Group Number" G defined as

$$G=3(1+0.276\,Re^{1/2}Sc^{1/3})LeN^{2/3}(R/s) \tag{6}$$

where Re is the local Reynolds number, Sc the Schmidt number, Le the Lewis number, N the total number of droplets in the cloud, R the average droplet radius, and s the average spacing between the centers of the droplets. With a decreasing group number, the combustion moves from external sheath combustion toward single droplet combustion. The present conditions under study lead to a group number of the order of 10 or higher, which puts the combustion in the external group combustion regime bordering on the external sheath combustion regime. This seems to be in agreement with the temperature distributions of Fig. 5. The hottest zone, which has a temperature of about 4000 K corresponding to stoichiometric conditions, forms a "sheath" around the oxygen-rich center region that has sonewhat lower temperatures (Fig. 5b). This flame envelope extends to a radius of about 0.2 cm maximum and 2 cm from the injector tip, or about the

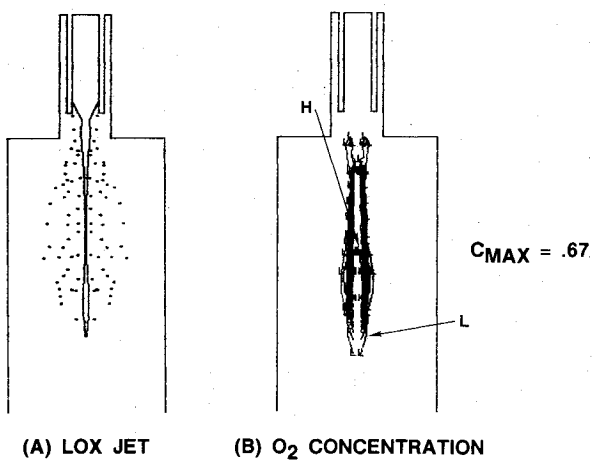

Fig. 4 Plots of liquid oxygen jet profile with spray and gaseous oxygen mass fraction contours (case I).

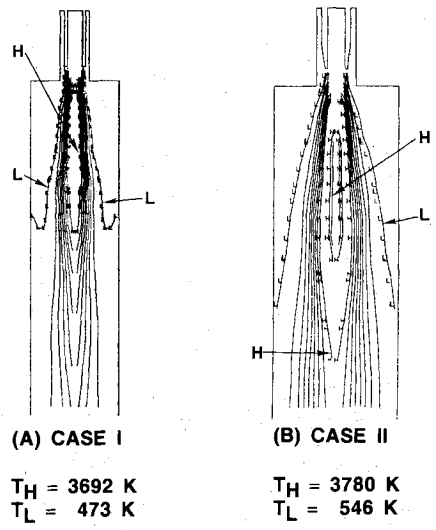

Fig. 5 Isotherm plots of flowfield, cases I and II (eight intervals between H and L).

same length as the liquid jet itself. The fact that few droplets exist beyond the tip of the liquid tip points to the short life span of the drops. Figures 6 and 7 give the contour maps of the OH and H_2O mass fractions respectively. The former may be taken as an indication of where the active chemistry is taking place. Outside of the OH zone, the primary process taking place is mixing rather than heat release. The H_2O plot reveals the sheath nature of the flame even more so than the isotherm plots. The maximum H_2O concentration of 0.88 means that the flame is near stoichiometric there and very fuel-rich elsewhere.

Figure 8 shows the axial profiles of the average droplet temperatures and sizes for cases I and II. It should be remembered that since ARICC is a real-time transient code and random distributions are used surrounding all drop-related properties, the instantaneous drop temperatures and sizes (even though averaged over the cross-sectional plane) fluctuate substantially. Thus a number of sample data are taken at various times, and what is plotted in Fig. 8 represents ensemble averages. Furthermore, since the drops vary greatly in size as they are heated to the critical temperature (154.6 K) while at the same time being "stripped," the instantaneous sizes plotted bear no simple relationship to the original sizes of the drops at their creation. They represent a balance between the size increase due to heating and the size decrease due to evaporation (breakup). However, the drop temperatures do reflect the gas temperatures in their immediate surroundings. Aside from the difference in liquid jet lengths, apparently the drops in case II experience greater heatup in the chamber as well as faster depletion after they are formed near the cup exit. Both of these can be attributed to the higher mixture ratio of case II that results in higher temperatures, larger flame zones, and higher accelerations of the gas stream. It may be noted that the steep upward slopes of the drop size curves in the cup region do not mean a rapid heatup. Rather, they refer to the increase in initial drop sizes as one moves from the inside of the cup to the outside, when the annular hydrogen gas stream experiences a sudden expansion and drop in velocity.

Figure 9 compares for case I the percentages of oxidizer that is atomized, vaporized, and reacted with similar predictions obtained using an older generation CICM[18] code. CICM is a single-phase code (no coupled liquid streams in the fluid dynamics) using very simple inviscid streamtube fluid dynamics and represents the state-of-the-art before the advent of modern computational fluid dynamics technology. Droplets are treated, but in an uncoupled fashion. Their agreement in the percent of liquid atomized is actually quite good. CICM's prediction of the percent vaporized, however, deviates substantially from that of ARICC and reflects a general time lag in the process after the drops are formed. This is because CICM contains no stripping evaporation model,

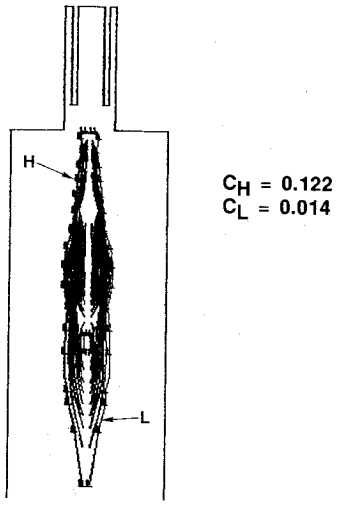

Fig. 6 Contour map of OH species mass fractions, case I (eight intervals between *H* and *L*).

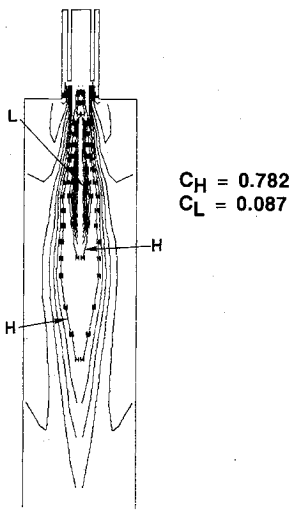

Fig. 7 Contour map of H_2O mass fractions, case I (eight intervals between *H* and *L*).

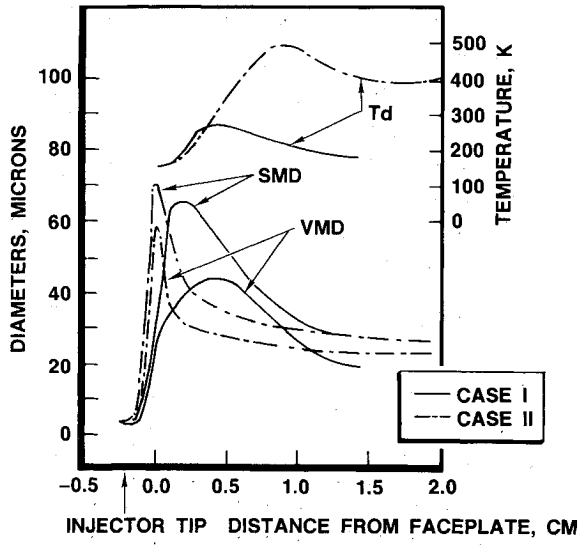

Fig. 8 Ensemble averages of droplet sauter mean diameter, volume mean diameter, and mass mean drop temperature (cases I and II).

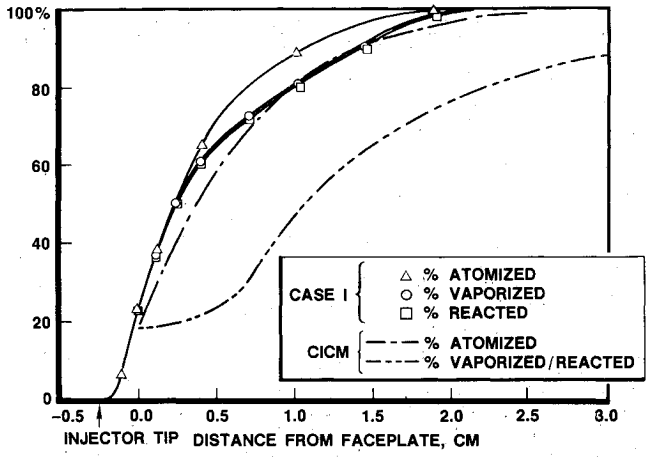

Fig. 9 Percentages of oxidizer atomized, vaporized, and reacted compared with CICM run (case I).

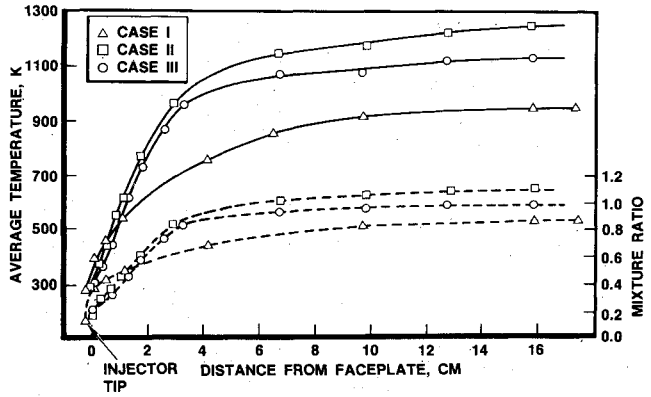

Fig. 10 Axial profiles of radially averaged temperatures and mixture ratios for three cases.

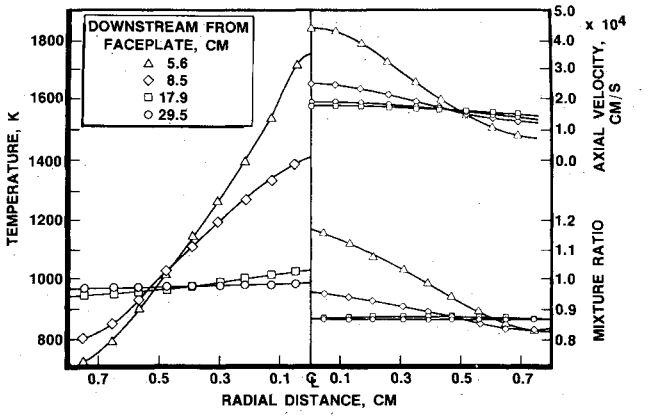

Fig. 11 Radial temperature, velocity, and mixture ratio profiles at various downstream locations (case I).

and the drops are heating while evaporating slowly through the diffusion-controlled process. The initial time lag is the droplet heatup period. Lastly, the fact that the percent vaporized and percent reacted curves are practically identical reflects the almost instantaneous nature of the combustion chemistry. This is realistic after estimates of the various time scales are considered. Thus, atomization is the primary rate-controlling step in the entire process, and vaporization secondarily so. ARICC, however, has a built-in capability to model slower chemistry with kinetic equations should the problem warrant it.

Mixing Characteristics

Finally, in Fig. 10, the mass-averaged cross-sectional temperature and mixture ratio are plotted vs the axial distance for all three cases. There is a close correlation between the two dependent variables. Judging from the initial steep-rise portion of the curves, it may be surmised that the combustion is essentially complete by about 3 cm, with a somewhat more diffused flame boundary for case I. From that point on, the dominant processes are viscous thermal, momentum, and species diffusion. These processes are clearly depicted in Fig. 11, where the radial profiles of temperature, axial velocity, and mixture ratios at four downstream locations are plotted for case I. Momentum and species diffusion seem to take place more rapidly than thermal diffusion. However, the mixing processes are essentially complete by about 18 cm. In Ref. 16, a hot-fire test has been reported for the case I conditions in which two kinds of brazed alloy wires that melt at 1,047 and 1,223 K respectively are placed at the 29.5-cm location. No melting was observed. Thermocouples located at the same vicinity measured a maximum temperature of about 920 K. These seem to be in harmony with the present ARICC predictions. More detailed measurements unfortunately are not available.

Conclusion

A realistic picture of the complex reacting flowfield inside the SSME fuel preburner has been produced using mechanistic numerical means. Far more detailed information than has been available with older theoretical models is generated. At least three different zones within the combustion chamber have been identified: an initial injection zone starting from inside the cup, closely tied to an external group diffusion combustion zone surrounded by cold unburnt fuel gas, and a large mixing zone for most of the length of the combustion chamber. Different physical processes dominate in each of the three zones.

While all major known physical mechanisms have been accounted for in the current model, much uncertainty still remains in the parameters and empirical coefficients used in the mathematical description of these physical models.[9] For instance, the identification of the atomization process as being the rate-controlling one points to the need to determine the atomization coefficients with greater certainty. Some of the unknowns, such as the supercritical LOX properties in a multispecies environment, simply await the careful measurements necessary to extend the range of our properties data. Others, such as the secondary droplet breakup criteria, would require the painstakingly detailed investigation of the physics itself, tackled in joint experimental and theoretical efforts. The ARICC code has been planned to be used to contribute in this aspect. Finally, as more nonintrusive hot-fire measurements of actual flowfield data can be made, greater confidence will be built concerning the absolute values of the predictions. As it now stands, the results are still more applicable to qualitative parametric investigations than to quantitative single-point predictions.

Acknowledgments

The work reported herein was sponsored by NASA/MSFC under Contract NAS8-27980.

References

[1]Przekwas, A. J., Singhal, A. K., and Tam, L. T., "Rocket Injector Anomalies Study," NASA CR-174702, Vols. 1 and 2, Aug. 1984.

[2]Harsha, P. T. and Edelman, R. B., "Analytical Modeling of Spray Diffusion Flame," AIAA Paper 84-1317, June 1984.

[3]Prakash, C., Singhal, A. K., and Shafer, C., "Thermofluid Analysis of the SSME Preburner Using a Gas-Gas Diffusion Model for Oxygen and Hydrogen Combustion at Supercritical Pressures," AIAA Paper 86-1425, June 1986.

[4]Liang, P. Y., "Liquid Rocket Combustor Computer Code Development," NASA CP-2372, *Proceedings of the High-Pressure Oxygen/Hydrogen Technology Conference*, June 1984, pp. 696-716.

[5]Liang, P. Y., Fisher, S., and Chang, Y. M., "Comprehensive Modeling of a Liquid Rocket Combustion Chamber," AIAA Paper 85-0232, Jan. 1985.

[6]Amsden, A. A., Ruppel, H. M., and Hirt, C. W., "SALE: A Simplified ALE Computer Program for Fluid Flow at all Flow Speeds," Rept. LA-8095, Los Alamos National Laboratory, Los Alamos, NM, June 1980.

[7]Faeth, G. M., "Spray Atomization and Combustion," AIAA Paper 86-0136, June 1986.

[8]Liang, P. Y., "Analysis of Coaxial Spray Combustion Flames and Related Numerical Issues," AIAA Paper 86-1511, June 1986.

[9]Liang, P. Y. and Jensen, R. J., "Modeling of Dense Sprays from LOX/H_2 Coaxial Injectors under Supercritical Conditions," *Proceedings of the 22nd JANNAF Combustion Meeting*, Oct. 1985.

[10]Faeth, G. M., Dominicis, D. P., Talpinsky J. F., and Olson, D. R., "Supercritical Bipropellant Droplet Combustion," *Proceedings of the 12th (International) Symposium on Combustion*, The Combustion Institute, July 1981, pp. 9-18.

[11]Williams, A., "Combustion of Droplets of Liquid Fuels: A Review," *Combustion and Flame*, Vol. 21, 1973, pp. 1-31.

[12]Dickerson, R. A. and Schuman, M. D., "Rate of Aerodynamic Atomization of Droplets," *Journal of Spacecraft and Rockets*, Vol. 2, Jan. 1965, pp. 99-100.

[13]Faeth, G. M., "Current Status of Droplet and Liquid Combustion," *Progress in Energy Combustion Science*, Vol 3, 1977, pp. 191-224.

[14]Ferrenberg, A. and Jaqua, V., "Atomization and Mixing Study—Part II," Rept. RI/RD83-170, NASA Contract NAS8-34504, Rockwell International/Rocketdyne Division, Canoga Park, CA, July 1983.

[15]Rabin, E. and Lawhead, R. B., "The Motion and Shattering of Burning and Non-burning Propellant Drops," AFOSR-TN-59-129, 1959.

[16]Lobitz, J., "Supporting Analysis Data—Preburner Design Definition," Rocketdyne SSME Phase CD Rept. RSS-8521-4, NASA Contract NAS8-26187, April 1971.

[17]Sirignano, W. A., "Fuel Droplet Vaporization and Spray Combustion Theory," *Progress in Energy Combustion Science*, Vol. 9, 1983, pp. 291-322.

[18]Sutton, R. D., Schuman, M. D., and Chadwick, W. D., "Operating Manual for Injection Combustion Model," NASA-CR-129031, April 1974.